Journal of Biomedical Optics

SPIEDigitalLibrary.org/jbo

Integrated optical microfluidic biosensor using a polycarbazole photodetector for point-of-care detection of hormonal compounds

Nuno Miguel Matos Pires
Tao Dong
Ulrik Hanke
Nils Hoivik

SPIE

Integrated optical microfluidic biosensor using a polycarbazole photodetector for point-of-care detection of hormonal compounds

Nuno Miguel Matos Pires, Tao Dong, Ulrik Hanke, and Nils Hoivik
Vestfold University College, Faculty of Technology and Maritime Sciences, Department of Micro and Nano Systems Technology, P.O. 2243, N-3103 Tonsberg, Norway

Abstract. A picogram-sensitive optical microfluidic biosensor using an integrated polycarbazole photodiode is developed. The photodetector is mainly composed of the blend heterojunction of poly [*N*-9′-heptadecanyl-2,7-carbazole-alt-5,5-(4′,7′-di-2-thienyl-2′,1′,3′-benzothiadiazole)] (PCDTBT) and [6,6]-phenyl C_{71}-butyric acid methyl ester ($PC_{70}BM$) and the poly(3,4-ethylenedioxythiophene):polystyrene sulfonate (PEDOT:PSS) as the hole transport layer. Analyte detection is accomplished via a chemiluminescent immunoassay performed in a poly(dimethylsiloxane)-gold-glass hybrid microchip, on which antibodies were immobilized and chemiluminescent horseradish peroxidase-luminol-peroxide reactions were generated. Enhanced sensor response to the chemiluminescent light is achieved by optimizing the thickness of PCDTBT: $PC_{70}BM$ and PEDOT:PSS. Using the optimized polycarbazole photodiode for detecting the human thyroid-stimulating hormone as the model target, the integrated biosensor demonstrates an excellent linearity in the range of 0.03 to 10 ng/ml with an analytical sensitivity of 68 pg/ml. The sensor response shows high specificity and reproducibility. Hormone detection in clinical samples is further demonstrated and compared with a commercial enzyme-linked immunosorbent assay. The integrated device reported here has potential to detect other hormonal compounds or protein targets. Moreover, the presented concept enables the development of miniaturized, low-cost but highly sensitive optical microfluidic biosensors based on integrated polymer photodetectors with high potential for point-of-care diagnostics. [DOI: 10.1117/1.JBO.18.9.097001]

Keywords: microfluidics; chemiluminescence; immunosensing; integrated optics; polymer photodetector; hormones; point-of-care.

Paper 130362R received May 22, 2013; revised manuscript received Jul. 30, 2013; accepted for publication Aug. 13, 2013; published online Sep. 3, 2013.

1 Introduction

Point-of-use measurement of analytes has attracted particular attention in fields of biomedical research and clinical diagnostics. Analysis of biomarkers or hormones on the spot could be especially valuable in diagnosis and risk analysis (e.g., patient response to cancer therapy, thyroid disease, genetic disorder).[1,2] Therefore, there is increasingly clinical relevance to develop point-of-care testing (POCT) devices that can shorten analysis time and provide more convenient test solutions compared to pre-existing laboratory methods. Among various analyte detection formats, immunoassay technology is widely employed in modern POCT devices for sensitive detection of disease-specific protein markers and pathogen infection–related markers.[3–5] Immunoassays involving antigen–antibody binding and analyte detection can be accomplished in minutes by the use of either optical or electrochemical methods.[6] Despite the wide use of electrochemical methods in POCT systems,[2,7] optical detection is still the preferred technique for clinical diagnostics due to the ubiquity of optical instrumentation in analytical laboratories.[8] Furthermore, optical components are well suited for miniaturized POCT immunoassay systems when integrated into self-contained microfluidic devices. Integrated optical microfluidic sensors are currently being developed to enhance the sensitivity, throughput, and portability of these systems.[9,10] However, the successful adoption of optical microfluidic devices for POCT purposes has yet to overcome challenges in integrating low-cost detectors into a single microchip.[11]

Among the optical methods of detection, chemiluminescence (CL) is particularly attractive for microfluidic POCT systems because of its simplicity and sensitivity.[12] The CL reaction acts as an internal light source, thereby reducing instrumentation complexity and background interference compared to fluorescence assays. CL-based methods have been successfully applied to on-chip immunoassays,[13,14] and therefore there is considerable interest in incorporating the CL scheme and optical detector into a single integrated analytical device.[15] The measurement of CL signals in microfluidic systems is typically conducted by externally mounted photomultiplier tubes,[16] charge-coupled devices[10] and microscope collection optics.[17,18] However, these off-chip devices do not translate to a truly POCT system due to their inherent complexity, high-cost, and high-power consumption.

Integrated silicon photodiodes and complementary metal-oxide-semiconductor (CMOS) image sensors have been used for microfluidic CL detection.[19] However, although both silicon- and CMOS-based sensors exhibit high detection sensitivities,[8] their fabrication is relatively complex which makes them too expensive to be incorporated on a POCT disposable device. The emergence of organic/polymer electronics has resulted in

Address all correspondence to: Tao Dong, Vestfold University College, Faculty of Technology and Maritime Sciences, Department of Micro and Nano Systems Technology, P.O. 2243, N-3103 Tonsberg, Norway. Tel: +4733037731; Fax: +4733031103; E-mail: tao.dong@hive.no

0091-3286/2013/$25.00

photodiodes that can be fabricated onto glass or flexible plastic substrates, using simple spin coating, inkjet printing, or spray coating techniques.[20] Besides having low-cost fabrication and small size, the organic photodiodes (OPDs) normally have flat geometry, with a typical total thickness <1 μm,[21] which makes them amenable to improved system integration. These advantages of the OPDs have motivated their application to compact microfluidic systems. Bilayer devices of copper phthalocyanine (CuPc) and fullerene (C_{60}) have been used for CL detection of hydrogen peroxide.[14,22] Other integrated microscale CL systems were developed using blend heterojunction photodiodes of poly(3-hexylthiophene) (P3HT) and [6,6]-phenyl-C_{61}-butyric acid methyl ester ($PC_{60}BM$),[23,24] demonstrating detection sensitivities in the micromolar range.[24]

The development of OPD-integrated microfluidic systems is still in a beginning stage. Further investigation may focus on developing OPDs with improved sensitivity. Recent advances in semiconducting polymers have brought novel photoactive materials with enhanced optoelectronic characteristics.[25] Among them, poly[*N*-9′-heptadecanyl-2,7-carbazole-alt-5,5-(4′,7′-di-2-thienyl-2′,1′,3′-benzothiadiazole)] (PCDTBT) form blend heterojunction devices exhibiting higher photon collection efficiencies and lower dark currents compared with P3HT-based photodiodes.[26] These unique characteristics may enhance the detection sensitivity of OPD microfluidic biosensors. Blend heterojunction devices of PCDTBT and fullerene derivatives were reported to be promising organic solar cells with superior power conversion efficiencies;[27] however, their higher sensitivity to light has not yet been exploited for microfluidic assays.

This work aims to establish a highly sensitive OPD-integrated microfluidic system, using a PCDTBT: $PC_{70}BM$ blend heterojunction device as an optical sensor for CL detection. The polycarbazole detector was fabricated on a glass slide and integrated with a microfluidic chip made mainly of poly (dimethylsiloxane) (PDMS).[28–30] The setup is amenable for miniaturized low-cost POCT applications. The developed OPD exhibited quantum efficiency of over 60% at 425 nm and a background current of a few picoamperes after sensor design optimization. With the optimized OPD, chemiluminescent immunoassays were performed within the integrated device for the detection of human thyroid-stimulating hormone (TSH), used as a model target analyte. TSH is an important biomarker associated with thyroid disease and stress disorders.[31] The integrated device reached detection sensitivities at the picogram level. Further, the device was validated using human serum samples.

2 Materials and Methods

2.1 *Chemicals and Reagents*

The polymers PCDTBT and $PC_{70}BM$ were obtained from Luminescence Technology Corp. (Taipei, Taiwan). Poly (3,4-ethylenedioxythiophene):polystyrene sulfonate (PEDOT: PSS, Baytron®P) was purchased as an aqueous dispersion from H.C. Starck Trading Company Ltd. (Shanghai, China). Indium tin oxide (ITO) deposited glass slides (thickness of ITO, 100 nm; surface sheet resistance, ~10 ohms/sq) were purchased from CSG Holding Co., Ltd. (Shenzhen, China). For the microfluidic chip, PDMS precursor and curing agent (Sylgard 184) were obtained from Dow Corning Holding Co., Ltd (Shanghai, China). *N*-[(3-trimethoxysilyl)propyl] ethylenediaminetriacetic acid, Na salt (TMS-EDTA; 50% in water) was supplied by IS Chemical Technology Ltd. (China); while (3-aminopropyl)-trimethoxysilane (APTMS; 97%) was from Sigma-Aldrich (St-Louis). SuperBlock™ phosphate-buffered saline (PBS, pH 7.2), *N*-ethyl-*N*′-(3-dimethylaminopropyl)-carbodiimide hydrochloride (EDC), *N*-hydroxysuccinimide (NHS), StartingBlock™ Blocking Buffer in PBS with 0.05% Tween-20, streptavidin horseradish peroxidase (HRP) conjugate, SuperSignal® ELISA femto luminol/enhancer solution and SuperSignal® ELISA femto stable peroxide solution were from Thermo Fisher Scientific (Shanghai, China). KeXing Biological technology Co. Ltd. (China) provided human TSH (recombinant) and its monoclonal antibody (mouse). Human tumor necrosis factor-alpha (TNF-α) and human interleukin-6 (IL-6) were supplied by Yapei Biotech. Ltd. (Shanghai, China) and Wuhan AmyJet Scientific Inc. (Wuhan, China), respectively. Polyclonal antiserum of TSH was obtained from an immunized mouse via traditional methods. After harvest, this antiserum was tested by standard dot-blot tests, which confirmed that no serious cross-reaction to the aforementioned monoclonal antibody has occurred. Biotinylation of the antiserum was conducted by Biotin Labeling Kit-NH_2 (Dojindo Laboratories, Kumamoto, Japan). Ultrapure water (18 MΩ/cm) was produced by a Milli-Q® system (Millipore, Milford) and used for all aqueous solutions and assay buffers.

2.2 *Device Description and Sensing Principle*

A scheme of the OPD-integrated microfluidic device is shown in Fig. 1(a). The device was formed by incorporating the polycarbazole photodetector comprising the ITO/PEDOT: PSS/PCDTBT: $PC_{70}BM$/LiF/Al diode architecture [Fig. 1(b)] to a hybrid microfluidic chip of PDMS/Au-coated glass. An active area of 0.16 cm^2 in the detector was aligned with a 30-μl volume reaction chamber on the hybrid microchip. This defined the detection zone where chemiluminescent sandwich immunoassays were developed on the Au surface. The Au-coated glass served as both a surface to immobilize antibodies and as a reflective backside substrate. The chemiluminescent oxidation of luminol by HRP labels in the presence of peroxide was used to generate ~425-nm light whose intensity was proportional to the amount of analyte targeted by the immunoassay. This light was transduced as a photocurrent signal by the OPD. Photons emitted in the CL reaction were absorbed by the PCDTBT: $PC_{70}BM$ blend heterojunction material, resulting in photogenerated electrons and holes collected at the corresponding opaque LiF/Al cathode and transparent ITO anode.

2.3 *Photodetector Preparation*

The polycarbazole detectors were prepared on ITO-coated glass substrates. After the substrates were pretreated by ultraviolet ozone, PEDOT:PSS (used as received) was deposited on top of the substrates via spin coating. The spin speed was varied between 1200 and 4500 rpm, resulting in film thicknesses ranging from 80 nm down to 25 nm. PCDTBT (used as received) was dissolved in chloroform to make 4 mg/ml solution, following by blending with $PC_{70}BM$ (used as received). The blends with a mass ratio of 1:4 in chloroform were then spin coated onto the PEDOT:PSS layer. The thickness of the resulting PCDTBT: $PC_{70}BM$ active layer ranged from 70 to 180 nm. An Ambios XP-100 profilometer was used to measure the

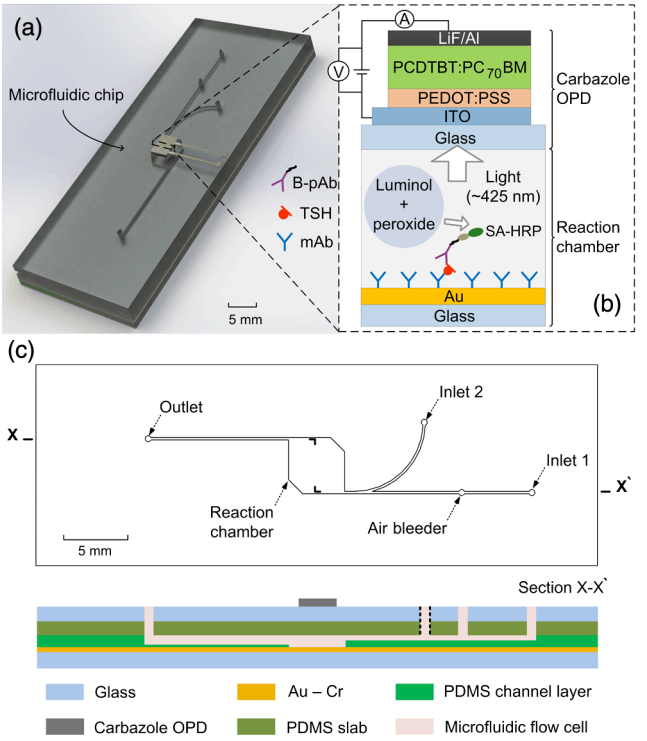

Fig. 1 Layout of the polycarbazole organic photodetector (OPD) integrated microfluidic device. (a) Three-dimensional scheme of the whole integrated device. The sensing area (4×4 mm^2) of the photodetector matches to the dimensions of the reaction chamber. (b) Polycarbazole diode design and sensing principle. A chemiluminescent immunoassay is employed to detect thyroid-stimulating hormone (TSH), with the generated light detected by the OPD. mAb, monoclonal antibody; B-pAb, biotinylated polyclonal antibody; SA-HRP, streptavidin-horseradish peroxidase conjugate. (c) Top view of the polydimethylsiloxane (PDMS) microchannel layer and side view of the OPD integrated microfluidic device (not to scale). The device is assembled by attaching the glass side of the OPD to the PDMS slab which is bonded to the PDMS-Au-glass hybrid microchip.

layer thicknesses. After deposition of the active layer, the substrates were transferred into a glove box filled with high-purity N_2 and dried at 60°C for 1 h. Furthermore, the LiF/Al electrode (~100 nm) was deposited onto the polymer film by thermal evaporation under a pressure of 3×10^{-4} Pa using a shadow mask. Following fabrication, the OPDs were encapsulated with a customized single-sided pressure-sensitive barrier foil. This ensures stability against oxygen and water vapor during device operation. Finished devices were diced into 25×52 mm slides.

2.4 *Microfluidic Setup and Chip Integration*

The microfluidic chip was fabricated by standard PDMS casting with a SU-8 master template.[32] A mixture of a Sylgard 184 precursor and a curing agent at a ratio of 10:1 (w/w) was degassed in a vacuum and poured onto the master template. After curing at 60°C for 1 h, the 800-μm thick PDMS cast was peeled off from the master and the structure of an 800-μm deep chamber was obtained using a scalpel blade. The microchannels connecting the inlets and chamber were 250-μm wide and 300-μm deep, whereas the channel connecting the outlet and chamber was 250-μm wide and 650-μm deep [Fig. 1(c)]. This microchannel layer was permanently attached to a 1-mm thick PDMS slab after exposing the contact surfaces to oxygen plasma.

The PDMS set was further attached to the Au-coated glass slide by means of carboxylamine coupling chemistry. A Pyrex 7740 glass wafer was previously sputtered with a 200-nm Au layer using a 20-nm Cr film as an adhesion layer. Prior to surface modification, the Au substrate was cleaned in 5:1 H_2SO_4/H_2O_2 solution, dried in a N_2 atmosphere, and exposed to UV ozone for 5 min. Clean substrate was immersed into a 10% (v/v) solution of TMS-EDTA in water for 2 h in order to develop carboxyl-terminated functional groups on the surface. After three washes with ultrapure water, the TMS-EDTA-modified substrate was subjected to 50-nM NHS and 200-mM EDC for 30 min at room temperature. The bonding surface of the PDMS chip was modified with amine-terminated groups after immersion in an ethanolic solution of 10% APTMS (v/v) for 1 h. The aminated substrate was then washed three times in ethanol. Both the modified PDMS and gold substrates were dried under N_2 for immediate bonding. The PDMS and Au surfaces were finally sealed at room temperature for 1 h. Irreversible attachment is achieved via NHS-EDC coupling chemistry. Also, the NHS-EDC functionalization of the Au surface within the reaction chamber allows covalent binding of antibody.[33]

Fluidic access holes were then added to the PDMS-Au hybrid microchip to create two channel inlets (750-μm wide), one air bleeder (750-μm wide) and one channel outlet (720-μm wide). For assembly of the integrated device, the glass side of the polycarbazole photodetector was permanently attached to the lid of the PDMS chip [Fig. 1(c)]. The glass substrate of the OPD also served as the world-to-chip interface; it was comprised of drilled access holes coinciding with the outlet, air bleeder, and inlets in the PDMS layer, whereby fluidic reservoirs were connected to the entrances of the microchannels. The reservoirs were polyether ether ketone (PEEK) capillary tubes (purchased from IDEX Health & Science, Shanghai, China) with 125-μm inner diameter (ID) and 510-μm outer diameter.

2.5 *CL Measurement and Immunoassay Procedure*

Figure 2 illustrates the experimental setup used for the CL measurements. A micro gear pump mzr®-4605 (IDEX

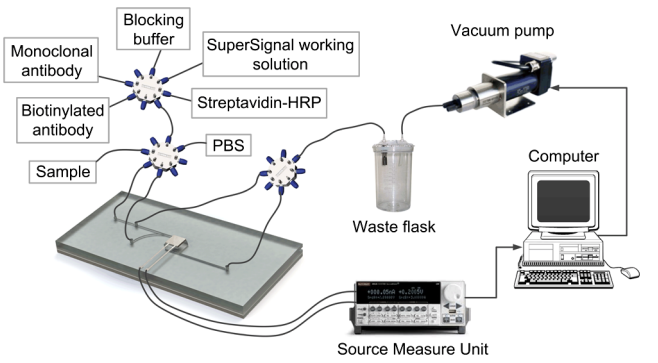

Fig. 2 Schematic of the experimental apparatus for the chemiluminescence (CL) immunoassay experiments. It shows the polycarbazole photodetector integrated microfluidic device connected to the readout equipment and fluid flow control system. The assay components are selectively delivered to the integrated device using external valves. HRP, horseradish peroxidase; PBS, phosphate-buffered saline. SuperSignal working solution represents the luminol/peroxide solution.

Trading Co. Ltd, Shanghai, China) operated by a PC was used to suck reagents into the OPD-integrated microfluidic device. The delivery of reagents was controlled by a valve system comprising three OMNIFIT© eight-way valves (Shanghai Beion Medical Technology Co., Ltd., China). Waste was collected by a vacuum flask connected to the pump through 762-μm ID PEEK tubing (IDEX). This tubing was also employed to connect the flask and reagent reservoirs to the corresponding OMNIFIT valve. On the other hand, the capillary reservoirs in the inlets, air bleeder, and an outlet of the integrated device were connected to the corresponding valve using 508-μm ID tubing. The air bleeder was used in this setup to remove small gas bubbles likely generated at the beginning stage of the reagent loading that may scatter the CL signal. During fluid flow operation, the pressure inside the flask generated by the pump did not exceed 50 kPa in all experiments. The photocurrent from the OPD was measured with a source measure unit (SMU, model 236, Keithley Instruments Inc., Cleveland, Ohio), and the recorded data were transferred to a PC via a USB-GPIB interface adapter (KUSB-488B, Keithley).

This setup was used for the CL immunoassay as depicted in Fig. 1(b). All assay components were prepared from 0.01-M PBS for immediate use. After the microchannels and reaction chamber were flushed with PBS, a 50-μl aliquot of 0.1-μg/ml anti-TSH monoclonal antibody was loaded into the chamber through the inlet 1 of the integrated device [Fig. 1(c)]. The pump was stopped after 90 s to allow the incubation of the antibody solution for 2 h within the chamber. The antibody was covalently immobilized to the chamber surface. After unbounded antibody was washed out from the microchip, the surface was blocked with StartingBlock™ blocking buffer and rinsed with PBS for 5 min. A 100-μl aliquot of a TSH standard solution was then added to the microchip via inlet 1. The content was incubated within the blocked chamber at room temperature for 15 min. Further, 100 μl of biotinylated polyclonal antibody was driven into the chip for 2 min; it was injected through inlet 2 to avoid contamination. Prior to use, the biotinylated antibody was purified by AllPrep™ protein procedure kit (Qiagen, Valencia). After the integrated device was rinsed with PBS, the immune complex interacted with streptavidin-HRP conjugate at concentrations ranging from 0.005 to 0.025 μg/ml. Subsequently, SuperSignal working solution, which was prepared by mixing equal parts of luminol/enhancer and stable peroxide solution, was transferred to the device via inlet 1 and was allowed to react with HRP. The light emitted in the CL reaction was thus detected by the OPD. All the assay experiments were performed in the dark. For the assay repetitions, the immune complex was dissociated using a glycine-HCl elution buffer (50 mM, pH 2.2) following the photocurrent measurement. The CL immunoassay was then restarted with the incubation of the TSH sample.

3 Results and Discussion

3.1 *Optimization of Photodetector Design*

Figure 3(a) shows the transient chemiluminescent signal of the polycarbazole detector for the detection of 10 ng/ml TSH. The first CL immunoassays were performed in 400-μl volume reservoirs made of PDMS that were attached between the Au substrate and the glass slide of the OPD. These reservoirs were held in place on the Au substrate using a poly(methylcrylate) holder.[34,35] The transient response of the OPD measured under short-circuit conditions was recorded from 0 to 10 min after the addition of the SuperSignal working solution. The signal reached a steady state within ~1 min.

The first set of CL measurements was conducted to optimize CL detection sensitivity of the polycarbazole detector. The sensitivity of OPD-based photodetection is enhanced by lowering dark current and increasing external quantum efficiency (EQE) for the desired wavelength range.[36] Optimizing the thickness of the active layer and hole transport layer represents a promising approach to the improvement of dark current and EQE characteristics of an OPD.[37,38] Thus, polycarbazole devices with varied PCDTBT: $PC_{70}BM$ and PEDOT:PSS thicknesses were fabricated in this work. Experimental optimization of the OPD design is conducted via comparison of dark current and EQE performance between the fabricated devices.

Photodetectors with active layers ranging from 70 to 180 nm were first compared. The PEDOT:PSS layer was fixed at 50 nm. Figure 3(a) plots the chemiluminescent signals measured with varied active layer thicknesses. The average photocurrent at the plateau of the signal (time period between 3 and 7 min) was determined for the comparison. A significant increase in the plateau current (I_p) was obtained for the PCDTBT: $PC_{70}BM$ thickness of 120 nm, which was approximately twofold higher than the 70-nm-thick layer. The changes in I_p were in agreement with the results for EQE [Fig. 3(b)]. Here, EQE was determined from the ratio of the current density collected at device electrodes to the flux density of incident photons:[39]

$$\mathrm{EQE} = \frac{hcJ_{sc}}{P_0 \lambda q} 100, \tag{1}$$

where J_{sc} represents the short-circuit current density, P_0 is the incident illumination in W/m^2, λ denotes the incident wavelength, and q is the elementary charge constant. The photocurrent was measured using a Keithley 236 SMU under monochromatic light irradiation provided by a TLS1509-X150 monochromatic light source (Zolix Instruments Co. Ltd., Beijing, China), equipped with a 150-W Xe lamp and an Omni-λ monochromator. The incident light power was calibrated using a Si photodiode (S6430-01, Hamamatsu Photonics K.K., Japan).

The EQE values were calculated for incident wavelengths between 400 and 500 nm at intervals of 5 nm. An EQE of 62% was obtained for the 120-nm-thick PCDTBT: $PC_{70}BM$ device under monochromatic light irradiation at 425 nm. The decreased responses observed in Fig. 3(b) for the PCDTBT: $PC_{70}BM$ thicknesses between 120 and 180 nm were mainly attributed to the reduced efficiency of charge transport in these thicker layers.[40] Figure 3(c) shows the background level (I_0) of the polycarbazole device as a function of the PEDOT:PSS thickness from 25 to 80 nm, where the PCDTBT: $PC_{70}BM$ layer was maintained at 120 nm. I_0 was measured before the assay components were added to the PDMS reservoirs such that only the effect from the dark current will be considered. A minimum background current was observed for the 40-nm-thick PEDOT:PSS when no bias voltage was applied, which corresponded to an approximately sixfold improvement over the layer thickness of 50 nm. I_p was also enhanced by the 40-nm-thick PEDOT:PSS [Fig. 3(d)]. The decreased thickness of PEDOT:PSS from 80 to 40 nm improved the detector response, which may have resulted from an increased EQE (Ref. 37) and/or an enhanced chemiluminescent light absorption by the OPD.

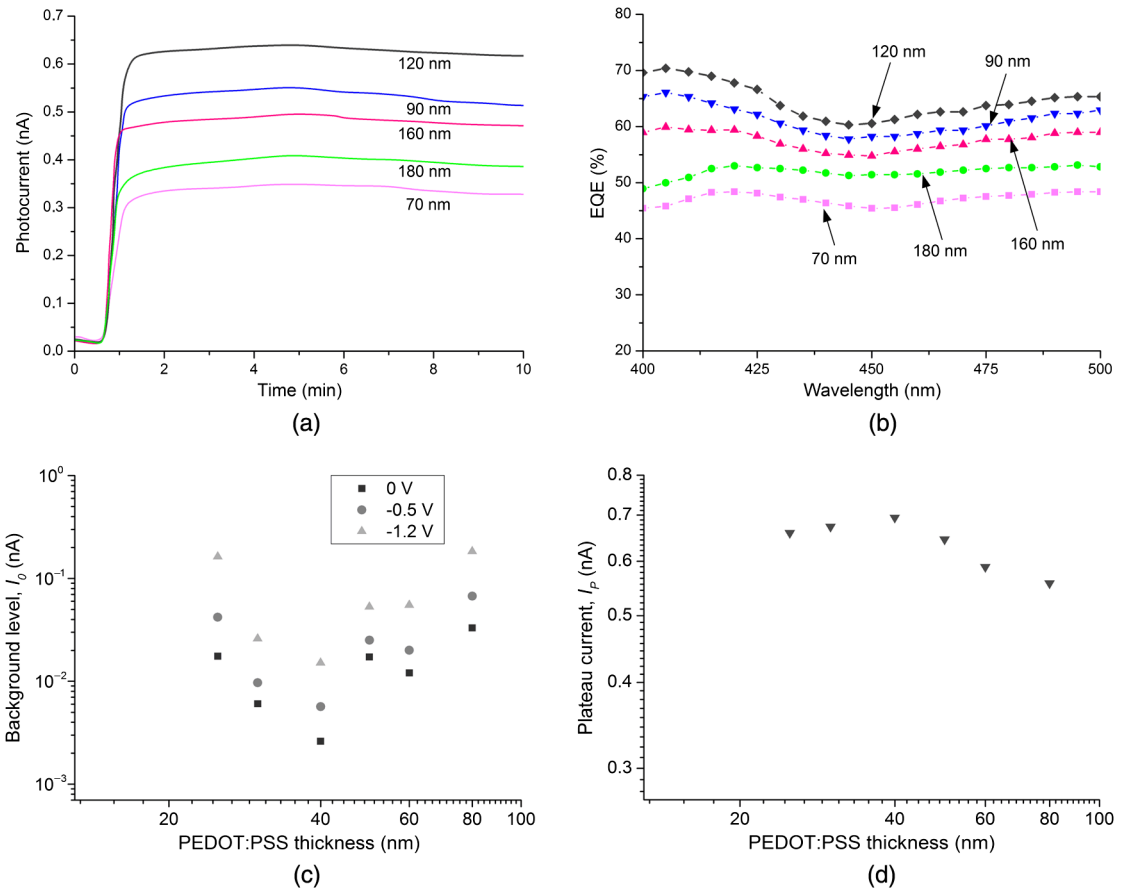

Fig. 3 Experimental optimization of the polycarbazole diode design. Polycarbazole devices with varied PCDTBT: $PC_{70}BM$ (photoactive layer) and PEDOT:PSS (hole transport layer) thicknesses were fabricated and tested. (a) Transient photocurrent response due to CL detection measured as a function of photoactive layer thickness. (b) External quantum efficiency (EQE) spectra for different PCDTBT: $PC_{70}BM$ thicknesses. (c) Background current measured at different bias voltages as a function of hole transport layer thickness. (d) Average photocurrent obtained from the plateau region of the transient response for different PEDOT:PSS thicknesses. The PEDOT:PSS was 50 nm in (a) and (b), whereas the PCDTBT: $PC_{70}BM$ was 120 nm in (c) and (d). The CL detection experiments for (a) and (d) were conducted with 10 ng/ml TSH.

3.2 *Optimization of Assay Conditions*

Further immunoassay tests were conducted with the optimized OPD comprising the 120-nm-thick PCDTBT: $PC_{70}BM$ and 40-nm-thick PEDOT:PSS. The OPD was integrated with the PDMS-Au hybrid microchip for the tests. The CL immunoassays performed within the integrated device were optimized before conducting quantitative TSH detection. Four concentrations of streptavidin-HRP conjugate were tested. The signal-to-noise ratio, defined here as the current ratio of I_p to I_0, was used for the analysis. Enhanced signal-to-noise ratio was encountered for a conjugate concentration of 15 ng/ml [Fig. 4(a)]. The results were consistent for four TSH concentrations. The optimized streptavidin-HRP concentration may have led to reduced shot noise of the detection system, which may be related to fluctuations in the photon flux density.[36] This noise is important for systems designed to detect low-magnitude photocurrents.

The influence of flow rate on photocurrent measurement was also analyzed. Immunoassays were conducted to determine the optimal flow conditions for the delivery of the SuperSignal working solution into the chip. An analyte concentration of 50 ng/ml was used for the tests. I_p was determined in independent experiments testing flow rates between 20 and 100 μl/min. The data in Fig. 4(b) indicated a decrease in I_p with decreasing flow rate values. The reduced CL signals might have been caused by insufficient time to complete the filling of the reaction chamber with the working solution before the signal plateau was reached (~1 min). Although flow rates of 80 and 100 μl/min led to enhanced photocurrent responses, the significant fluctuations found in the CL signals prevented the use of these flow rates for later experiments. Thus, a flow rate of 55 μl/min was found to be optimal as it provided an ideal compromise between high photocurrent response and signal stability. Notably, no fluid leakage was encountered even at the highest flow rate, indicating the robustness of the OPD-integrated microfluidic device.

3.3 *Quantitative Detection Tests*

Quantitative CL immunoassay detection was conducted under optimal conditions as described above. Figure 5(a) shows the current–voltage curves of the various TSH concentrations prepared in PBS. The photocurrent data were determined from the plateau region of the chemiluminescent signal by applying a range of bias voltages to the OPD. Upon incubation of the integrated device with TSH, the photocurrent remarkably changed with cortisol concentration. The photocurrent from the detected 5 ng/ml analyte was ~100-fold higher than that from a nonanalyte concentration. The current measurements were limited to short-circuit conditions to ensure minimum background levels

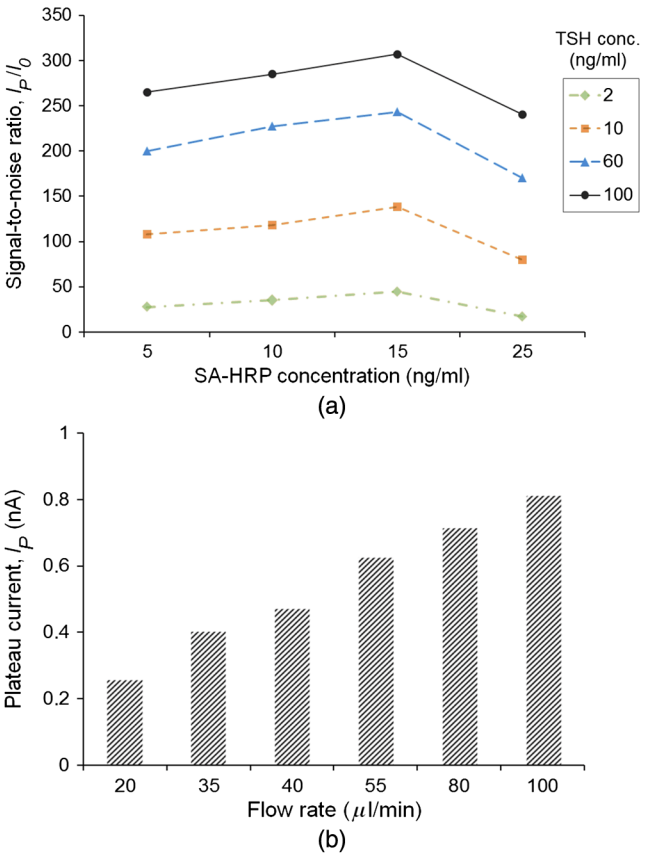

Fig. 4 Optimization of assay conditions for the microfluidic CL detection. (a) Signal-to-noise ratio of the polycarbazole photodetector integrated microfluidic device for a range of streptavidin-horseradish peroxidase conjugate (SA-HRP) concentrations. Four concentrations of TSH were used for the analysis. (b) Detection of 50 ng/ml TSH varying the volumetric flow rate used for delivery of luminol/peroxide solution into the integrated device.

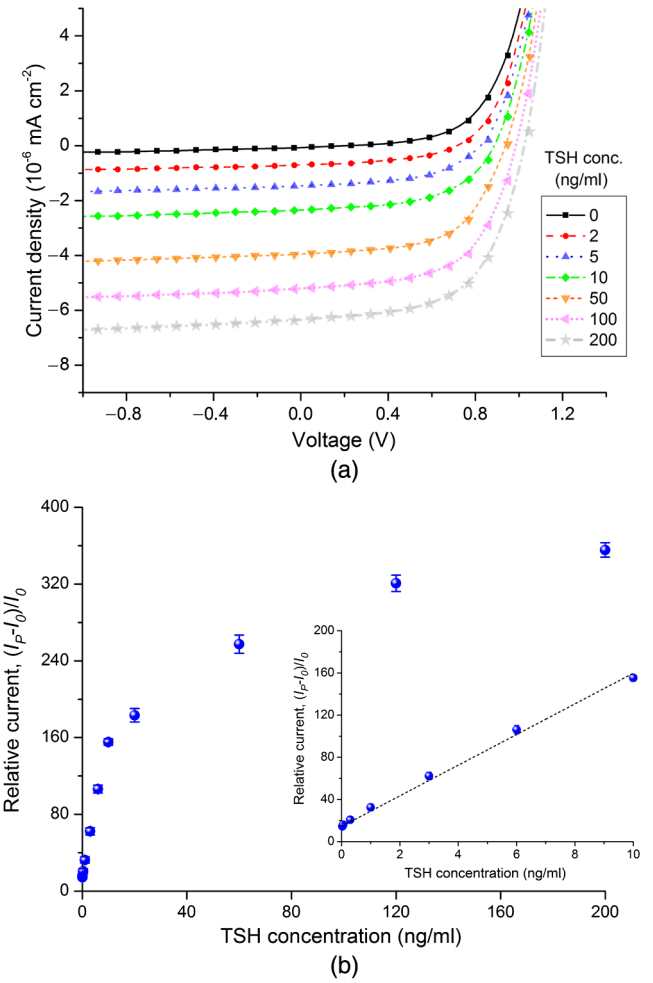

Fig. 5 Quantitative CL immunoassay detection of TSH. (a) Current-voltage profiles at different TSH concentrations. (b) Calibration curve obtained from the normalized photocurrent for a range of TSH concentrations in phosphate-buffered saline. Inset represents the linear region of the calibration curve. All measurements of current in (b) were conducted with no bias applied. The error bars represent standard deviation for triplicate assays.

[Fig. 3(c)] in further quantitative detection tests. To determine the calibration curve, the photocurrent data were normalized by plotting $[(I_p - I_0)/I_0]$ against the TSH concentration [Fig. 5(b)]. Linearity was found in the range of 0.03 to 10 ng/ml with a correlation coefficient of 0.995. The analytical sensitivity, determined from the slope of the linear region, was ~68 pg/ml. The detection limit is estimated to be <30 pg/ml as indicated by the result of 3× standard deviation of five blank measurements. This result is below the 500 pg/ml lowest limit reported for a P3HT OPD-based optical biosensor.[23] The analytical performance of the integrated device is dependent upon the sensitivity of the OPD. Further decrease in dark current may be achieved by reducing the photoactive area.[22] However, this may imply reduction in the dimensions of the reaction chamber and consequently the quantity of luminol/peroxide working solution for the analysis. A decrease in light intensity generated by the CL reaction will result in a reduced photocurrent response by the OPD.

3.4 *Specificity and Reproducibility Tests*

The specificity of the method was tested using various reagent blanks, cytokines TNF-α and IL-6 as negative controls and 2 ng/ml TSH as a positive control. The anti-TSH monoclonal antibody, blocking buffer, streptavidin-HRP conjugate and luminol/peroxide working solution were used for the reagent blanks. Figure 6 plots the results of the specificity tests. No distinguishable interference from any of the prepared blanks on the photocurrent measurements was observed. Furthermore, the variation of photocurrent for TNF-α and IL-6, biomarkers also related with thyroid disease and stress disorders,[31,41] was negligible compared with TSH.

The CL assay variability was also characterized. Intra-assay variability, obtained from the relative standard deviation, was calculated from the five assay repetitions for 2 ng/ml TSH concentration using two polycarbazole devices prepared in the same batch. Inter-assay variability was determined in the same way as intra-assay variability but testing three OPDs prepared in three batches. The values inferior to 3% and 7% for intra-assay and inter-assay, respectively, indicated good detection reproducibility of the developed microfluidic system.

3.5 *Analysis of Clinical Samples*

The analysis of complex biological samples is commonly conducted to further evaluate the feasibility of a biosensor

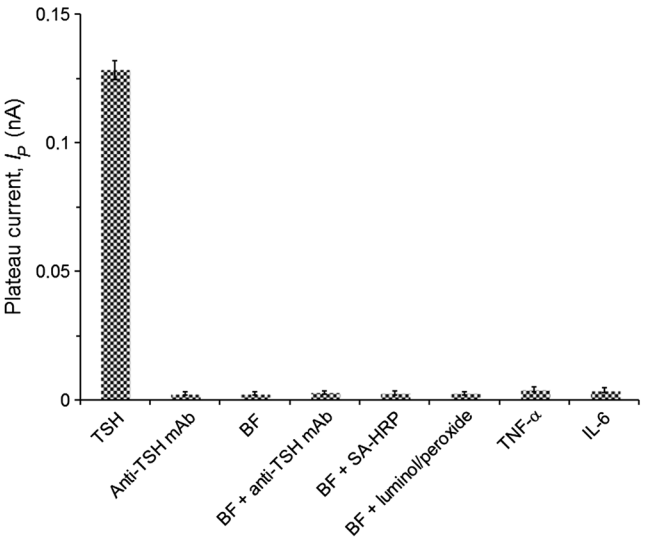

Fig. 6 Specific detection of TSH by the polycarbazole photodetector integrated microfluidic device. The specificity tests were performed with respect to various reagent blanks, analyzing the interference from monoclonal antibody (mAb), blocking buffer (BF), streptavidin-horseradish peroxidase conjugate (SA-HRP) and luminol/peroxide working solution. The negative controls were the cytokines human tumor necrosis factor-alpha (TNF-α) and human interleukin-6 (IL-6) while the positive control was 2 ng/ml TSH. The error bars represent standard deviation for triplicate tests.

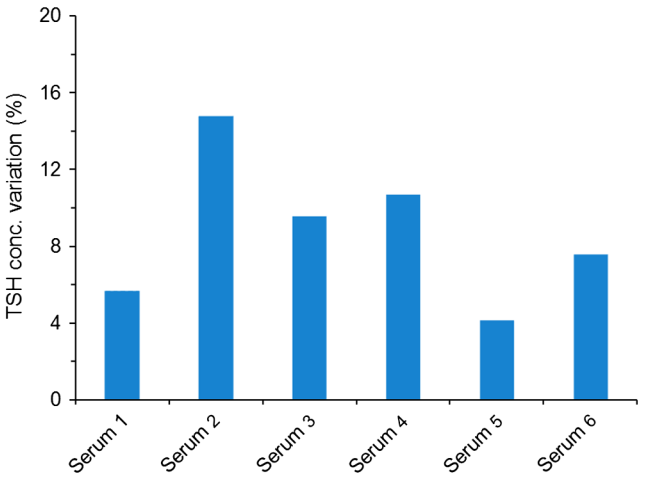

Fig. 7 Absolute percentage variation in six serum concentrations of TSH detected by two methods. Each variation value was obtained from the ratio of the TSH concentration estimated with the polycarbazole photodetector integrated microfluidic device to that detected using a standard enzyme-linked immunosorbent assay method.

system.[42–44] To investigate the feasibility of the developed OPD-integrated microfluidic device for POCT applications, six serum samples of adult subjects were tested in parallel with six devices. The TSH levels in the serum samples were within the range of 0.035 to 0.12 ng/ml as detected by a commercially available enzyme-linked immunosorbent assay (ELISA) method (Abcam®, Cambridge). All tests were conducted with 100 μl of diluted serum. The procedures for the commercial ELISA including assay preparation and sample dilution were performed according to the instructions of the manufacturer.

Upon incubation of the integrated devices with the corresponding diluted serum samples, the measured photocurrents were normalized via $[(I_p - I_0)/I_0]$ and the TSH levels were thus estimated using the calibration curve shown in Fig. 5(b). The estimated concentrations were then compared with those obtained with commercial ELISA. To this end, the absolute percentage difference in TSH concentration between the two methods of detection was determined and plotted for each serum sample (Fig. 7). This difference did not exceed 15% which indicated good correlation between the measurements by the integrated device and those made by ELISA.

The integrated device is originally designed and developed for single use. The low cost of both the PDMS-Au hybrid microchip and polycarbazole OPD ensures feasibility of a POCT disposable device. In addition, the PDMS microfluidic substrate guarantees sufficient assay miniaturization and reduction of reagent consumption. Most POCT applications typically demand fast sample analysis.[45] The analyte detection described in this study required 15 min for incubation of a sample and then 1 min for equilibration with luminol/peroxide working solution. A reduction in sample incubation time could be an immediate solution to further decrease the overall duration of the detection process.

4 Conclusion and Outlook

A novel OPD-integrated microfluidic biosensor was developed for the point-of-use detection of clinically relevant protein analytes. The biosensor exploited the use of the PCDTBT: $PC_{70}BM$ blend heterojunction OPD as a highly sensitive optical detector for CL immunoassays. This OPD was constructed with the ITO/PEDOT: PSS/PCDTBT: $PC_{70}BM$/LiF/Al structure, the optimized design of which comprised the PCDTBT: $PC_{70}BM$ and PEDOT:PSS thicknesses of 120 and 40 nm, respectively. Using TSH as the model target for the assays, the integrated optical biosensor exhibited a linear response of four orders of magnitude, with an analytical sensitivity in approximately tens of picograms per milliliter. Moreover, the integrated system showed high detection reproducibility and specificity. The feasibility for analysis of complex biological samples was also demonstrated. The results shown in this study suggested that the polycarbazole OPDs may be promising for integrated optical microfluidic biosensors. The concept presented here could also stimulate the development of POCT systems with retaining adequate sensitivity, cost, and compactness. Further, the concept may be applicable to other protein analytes using other antibodies.

The performance tests described in this work have employed relatively laborious assays and external fluid control components. In the future work, a fully autonomous microfluidic device would be realized by incorporating microstructures for on-chip reagent storage and passive fluid delivery. The study of simpler CL-based immunoassays for future POCT devices will also be considered. Furthermore, the OPD-integrated microfluidic biosensor could be expanded to a multiplex platform in which tens of hormones or other proteins could be detected in a single sample. This would offer a promising approach for the fields of on-the-spot analysis and clinical diagnostics.

Acknowledgments

This work was mainly supported by Norsk regional kvalifiseringsstøtte fra Oslofjorfondet (Et cellebasert digitalt mikrofluidisk system, project no. 220635; Mikrofluidisk

plattform integrert med lavkostnads fotodetektorer, proj. no: 229857). Research Council of Norway is acknowledged for the support to the Norwegian Micro- and Nano-Fabrication Facility, NorFab (197411/V30), Norwegian long term support from NorFab (Fabrication of nano-refinery for biomedical applications; Microfabrication of biocompatible materials and surface treatments for living-cell-based lab-on-chip devices). The authors thank School of Mechanical Engineering in Nanjing University of Science & Technology and Institute of Hydrobiology in Chinese Academy of Sciences for arranging the experimental activities and covering part of their costs.

References

1. F. S. Ligler, "Perspective on optical biosensors and integrated sensor systems," *Anal. Chem.* **81**(2), 519–526 (2009).
2. A. Warsinke, "Point-of-care testing of proteins," *Anal. Bioanal. Chem.* **393**(5), 1393–1405 (2009).
3. J. S. Ahn et al., "Development of a point-of-care assay system for high-sensitivity C-reactive protein in whole blood," *Clin. Chim. Acta* **332**(1–2), 51–59 (2003).
4. P.-Y. Chung et al., "Amplification-free point of care immunosensor for detecting type V collagen at a concentration level of ng/ml," *Proc. SPIE* **8029**, 80291C (2011).
5. V. Gubala et al., "Point of care diagnostics: status and future," *Anal. Chem.* **84**(2), 487–515 (2012).
6. A. Bange, H. B. Halsall, and W. R. Heineman, "Microfluidic immunosensor systems," *Biosens. Bioelectron.* **20**(12), 2488–2503 (2005).
7. N. M. M. Pires et al., "A mediator embedded micro-immunosensing unit for electrochemical detection on viruses within physiological saline media," *J. Micromech. Microeng.* **21**(11), 115031 (2011).
8. F. B. Myers and L. P. Lee, "Innovations in optical microfluidic technologies for point-of-care diagnostics," *Lab Chip* **8**(12), 2015–2031 (2008).
9. C. Monat, P. Domachuk, and B. J. Eggleton, "Integrated optofluidics: a new river of light," *Nat. Photonics* **1**(2), 106–114 (2007).
10. M. Yang et al., "An automated point-of-care system for immunodetection of staphylococcal enterotoxin B," *Anal. Biochem.* **416**(1), 74–81 (2011).
11. C. D. Chin, V. Linder, and S. K. Sia, "Commercialization of microfluidic point-of-care diagnostic devices," *Lab Chip* **12**(12), 2118–2134 (2012).
12. A. Bhattacharyya and C. M. Klapperich, "Design and testing of a disposable microfluidic chemiluminescent immunoassay for disease biomarkers in human serum samples," *Biomed. Microdevices* **9**(2), 245–251 (2007).
13. J. Yakovleva et al., "Microfluidic enzyme immunoassay using silicon microchip with immobilized antibodies and chemiluminescence detection," *Anal. Chem.* **74**(13), 2994–3004 (2002).
14. M. Miyake et al., "Performance of an organic photodiode as an optical detector and its application to fluorometric flow-immunoassay for IgA," *Talanta* **96**, 132–139 (2012).
15. X. Wang et al., "Integrated thin-film polymer/fullerene photodetectors for on-chip microfluidic chemiluminescence detection," *Lab Chip* **7**(1), 58–63 (2007).
16. X. Huang and J. Ren, "On-line chemiluminescence detection for isoelectric focusing of heme proteins on microchips," *Electrophoresis* **26**(19), 3595–3601 (2005).
17. C. Chandsawangbhuwana et al., "High-throughput optofluidic system for the laser microsurgery of oocytes," *J. Biomed. Opt.* **17**(1), 015001 (2012).
18. T. Dong et al., "Integratable non-clogging microconcentrator based on counter-flow principle for continuous enrichment of CaSki cells sample," *Microfluid. Nanofluid.* **10**(4), 855–865 (2011).
19. B. Kuswandi et al., "Optical sensing systems for microfluidic devices: a review," *Anal. Chim. Acta* **601**(2), 141–155 (2007).
20. M. Granstrom et al., "Laminated fabrication of polymeric photovoltaic diodes," *Nature* **395**(6699), 257–260 (1998).
21. E. Kraker et al., "Integrated organic electronic based optochemical sensors using polarization filters," *Appl. Phys. Lett.* **92**(3), 033302 (2008).
22. O. Hofmann et al., "Thin-film organic photodiodes as integrated detectors for microscale chemiluminescence assays," *Sens. Actuators B Chem.* **106**(2), 878–884 (2005).
23. J. R. Wojciechowski et al., "Organic photodiodes for biosensors miniaturization," *Anal. Chem.* **81**(9), 3455–3461 (2009).
24. X. Wang et al., "Thin-film organic photodiodes for integrated on-chip chemiluminescence detection - application to antioxidant capacity screening," *Sens. Actuators B Chem.* **140**(2), 643–648 (2009).
25. A. J. Heeger, "Semiconducting polymers: the Third Generation," *Chem. Soc. Rev.* **39**(7), 2354–2371 (2010).
26. S. H. Park et al., "Bulk heterojunction solar cells with internal quantum efficiency approaching 100%," *Nat. Photonics* **3**(5), 297–302 (2009).
27. K. K. H. Chan et al., "Charge injection and transport studies of poly(2,7-carbazole) copolymer PCDTBT and their relationship to solar cell performance," *Org. Electron.* **13**(5), 850–855 (2012).
28. J. Nichols et al., "On-chip digital microfluidic architectures for enhanced actuation and sensing," *J. Biomed. Opt.* **17**(6), 067005 (2012).
29. K. W. Kho et al., "Polymer-based microfluidics with surface-enhanced Raman-spectroscopy-active periodic metal nanostructures for biofluid analysis," *J. Biomed. Opt.* **13**(5), 054026 (2008).
30. T. Dong et al., "A smart fully integrated micromachined separator with soft magnetic micro-pillar arrays for cell isolation," *J. Micromech. Microeng.* **20**(11), 115021 (2010).
31. G. P. Chrousos, "Stress and disorders of the stress system," *Nat. Rev. Endocrinol.* **5**(7), 374–381 (2009).
32. J. Wu and M. Gu, "Microfluidic sensing: state of the art fabrication and detection techniques," *J. Biomed. Opt.* **16**(8), 080901 (2011).
33. E. Ouellet et al., "Novel carboxyl-amine bonding methods for poly (dimethylsiloxane)-based devices," *Langmuir* **26**(14), 11609–11614 (2010).
34. B. Xiao et al., "Integrated micro Pirani gauge based hermetical package monitoring for uncooled VOx bolometer FPAs," *Microsyst. Technol.* **17**(1), 115–124 (2011).
35. X. Zhao et al., "Compatible immune-NASBA LOC device for quantitative detection of waterborne pathogens: design and validation," *Lab Chip* **12**(3), 602–612 (2012).
36. J. Huang and J. deMello, "An introduction to organic photodetectors," Chapter 6 in *Organic Electronics in Sensors and Biotechnology*, R. Shinar and J. Shinar, Eds., pp. 193–263, McGraw-Hill, New York (2009).
37. B. Friedel et al., "Effect of layer thickness and annealing of PEDOT:PSS layers in organic photodetectors," *Macromolecules* **42**(17), 6741–6747 (2009).
38. B. V. Andersson et al., "An optical spacer is no panacea for light collection in organic solar cells," *Appl. Phys. Lett.* **94**(4), 043302 (2009).
39. A. J. Moulé and K. Meerholz, "Intensity-dependent photocurrent generation at the anode in bulk-heterojunction solar cells," *Appl. Phys. B* **92**(2), 209–218 (2008).
40. T.-Y. Chu et al., "Highly efficient polycarbazole-based organic photovoltaic devices," *Appl. Phys. Lett.* **95**(6), 063304 (2009).
41. A. G. Gianoukakis, N. Khadavi, and T. J. Smith, "Cytokines, Gravés disease, and thyroid-associated ophthalmopathy," *Thyroid* **18**(9), 953–958 (2008).
42. L. Zhang and T. Dong, "A Si/SiGe quantum well based biosensor for direct analysis of exothermic biochemical reaction," *J. Micromech. Microeng.* **23**(4), 045011 (2013).
43. P. Yager et al., "Microfluidic diagnostic technologies for global public health," *Nature* **442**(7101), 412–418 (2006).
44. X. Zhao and T. Dong, "Multifunctional sample preparation kit and on-chip quantitative nucleic acid sequence-based amplification tests for microbial detection," *Anal. Chem.* **84**(20), 8541–8548 (2012).
45. T. Laksanasopin et al., "Microfluidic point-of-care diagnostics for resource-poor environments," *Proc. SPIE* **7318**, 73180E (2009).